Eric J. Rainis
Musculoskeletal Research Center,
Department of Bioengineering,
University of Pittsburgh,
Pittsburgh, PA 15219

Steve A. Maas

Heath B. Henninger

Musculoskeletal Research Laboratories,
Department of Bioengineering,
and Scientific Computing and Imaging Institute,
University of Utah,
Salt Lake City, UT 84112

Patrick J. McMahon
Musculoskeletal Research Center,
Department of Bioengineering,
University of Pittsburgh,
Pittsburgh, PA 15219

Jeffrey A. Weiss
Musculoskeletal Research Laboratories,
Department of Bioengineering,
and Scientific Computing and Imaging Institute,
University of Utah,
Salt Lake City, UT 84112

Richard E. Debski
Ph.D.
Musculoskeletal Research Center,
Department of Bioengineering,
University of Pittsburgh,
Pittsburgh, PA 15219
e-mail: genesis1@pitt.edu

Material Properties of the Axillary Pouch of the Glenohumeral Capsule: Is Isotropic Material Symmetry Appropriate?

Inconclusive findings regarding the collagen fiber architecture and the material properties of the glenohumeral capsule make it unclear whether the material symmetry of the glenohumeral capsule is isotropic or anisotropic. The overall objective of this work was to use a combined experimental and computational protocol to characterize the mechanical properties of the axillary pouch of the glenohumeral capsule and to determine the appropriate material symmetry. Two perpendicular tensile and finite simple shear deformations were applied to a series of tissue samples from the axillary pouch of the glenohumeral capsule. An inverse finite element optimization routine was then used to determine the material coefficients for an isotropic hyperelastic constitutive model by simulating the experimental conditions. There were no significant differences between the material coefficients obtained from the two perpendicular tensile deformations or finite simple shear deformations. Furthermore, stress-stretch relationships predicted by utilizing the material coefficients from one direction were able to predict the responses of the same tissue sample in the perpendicular direction. These similarities between the longitudinal and transverse material behaviors of the tissue imply that the capsule may be considered an isotropic material. However, differences did exist between the material coefficients obtained from the tensile and shear loading conditions. Therefore, a more advanced constitutive model is needed to predict both the tensile and shear responses of the material. [DOI: 10.1115/1.3005169]

Introduction

The glenohumeral capsule is a complex sheet of fibrous tissue composed of several variably thick regions (superior glenohumeral ligament, middle glenohumeral ligament, anterior and posterior bands of the inferior glenohumeral ligament (IGHL), and the axillary pouch) that function collectively to stabilize the shoulder in extreme ranges of motion (Fig. 1) [1,2]. Specifically, the axillary pouch of the IGHL is the primary stabilizer when the joint is placed in abduction and external rotation—the position in which joint dislocations occur most frequently. Previously, these regions have been treated as discrete uniaxial ligaments [3–7]. However, recent experimental data have suggested that the capsule functions more like a fibrous sheet of tissue, as the strain [8,9] and force [10] distributions are multiaxial and not aligned with the longitudinal direction of these regions. These multiaxial strain distributions may be attributed to the complex deformations that the capsule undergoes as it wraps around the articular surface of the humeral head.

Contributed by the Bioengineering Division of ASME for publication in the JOURNAL OF BIOMECHANICAL ENGINEERING. Manuscript received October 22, 2007; final manuscript received August 18, 2008; published online January 6, 2009. Review conducted by Jacques M. Huyghe.

The material and structural properties of each region of the capsule have been evaluated extensively in the direction parallel to its longitudinal axis [11–17] but the material response of the capsule along other directions remains largely unknown. Previous studies have evaluated the material properties of this tissue in two perpendicular directions utilizing dog-bone tissue samples [18,19]. The preparation of these tissue samples may have removed important collagen fiber interactions along their edges. These interactions might not have been severed in a reproducible manner between tissue samples and affected the resulting material properties. Moreover, discrepancies exist regarding the collagen fiber organization of the axillary pouch, with one study reporting a clear axis of collagen fiber alignment [20] while others found a certain level of disorganization [21,22]. These discrepancies make it unclear whether the material symmetry of the tissue is best described as isotropic or anisotropic. In addition, these studies have primarily determined the mechanical response of the tissue in the linear region of the stress-strain curve. However, the response of the tissue throughout the entire stress-strain curve is important for the functional role of the capsule, especially since the ligaments are typical only loaded into the toe region of the stress-strain curve during normal activities.

The objective of this study was to characterize the material properties of the axillary pouch of the glenohumeral capsule in

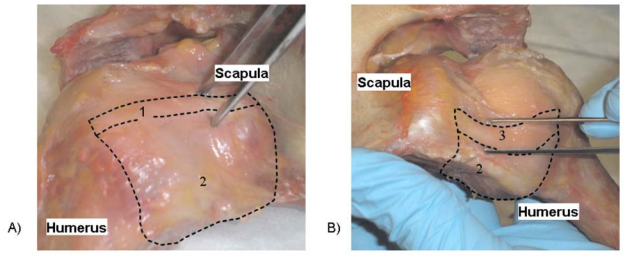

Fig. 1 (*a*) Anterior and (*b*) posterior view of the glenohumeral capsule. The following structures are shown: (1) anterior band, (2) axillary pouch, and (3) posterior band of the inferior glenohumeral ligament.

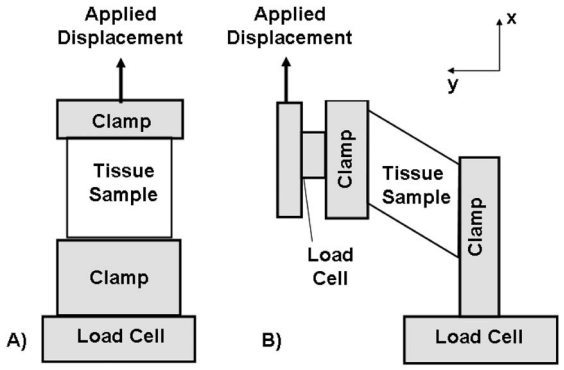

Fig. 2 Mechanical testing setup for (*a*) tensile and (*b*) shear loading conditions showing the load cell and clamp relationships

response to tensile and shear elongations. It was hypothesized that because the collagen fiber architecture is relatively disorganized overall and there is little difference in certain material properties between two perpendicular directions, isotropic material symmetry would effectively describe the function of the glenohumeral capsule. High rates of redislocation exist following the current treatment for injuries sustained during the initial dislocation episode. Therefore, characterization of the structure of the glenohumeral capsule could lead to new biomechanically based strategies to improve diagnostic exams and surgical repair protocols following shoulder dislocation.

Methods

A combined experimental-computational protocol was used to characterize the axillary pouch of the glenohumeral capsule. Experimentally, two perpendicular tensile and shear elongations were applied to the tissue sample, while the clamp reaction force and clamp displacement were recorded. These values were then used in an inverse finite element optimization routine to simulate the experimental conditions, optimizing the material coefficients until the sum-of-squares difference between the load-elongation curves from experimental measurements and computational predictions was minimized.

Material Testing. Ten fresh-frozen cadaveric shoulders (donor age 51 ± 8 years) were stored at $-20\,^{\circ}\mathrm{C}$ and then thawed for 24 h at room temperature prior to testing. The shoulders were then dissected free of all skin and musculature, and tissue samples from the axillary pouch of the glenohumeral capsule were obtained using a cutting guide and scalpel to form square sheets (25×25 mm^2). Each joint was examined and determined to be free of osteoarthritis and any visible signs of previous injury. Range of motion was also assessed prior to dissection, and any specimens exhibiting signs of joint contracture were excluded from the study.

The tissue samples were hydrated using physiological saline solution throughout the entire testing protocol. The superior margin of the anterior band of the inferior glenohumeral ligament (AB-IGHL) was used as an anatomical reference to define the transverse (perpendicular to the longitudinal axis of the AB-IGHL) and longitudinal (parallel to the longitudinal axis of the AB-IGHL) loading directions during mechanical testing. To identify the AB-IGHL, the joint was distracted and external rotation was applied while the PB-IGHL was identified with the joint distracted and internally rotated. Tissue samples of the axillary pouch were then extracted from the region between the AB-IGHL and PB-IGHL before loading conditions were applied.

A total of four nondestructive loading conditions were used in this protocol: (1) tensile elongation applied in the direction parallel to the longitudinal axes of the AB-IGHL (tensile longitudinal), (2) tensile elongation applied in the direction perpendicular to the longitudinal axes of the AB-IGHL (tensile transverse), (3) shear elongation applied in the direction parallel to the longitudinal axes of the AB-IGHL (shear longitudinal), and (4) shear elongation applied in the direction perpendicular to the longitudinal axes of the AB-IGHL (shear transverse). The testing order was randomized to minimize the effect of order on the results, and preliminary tests were performed to assess this issue. A loading condition was applied to a tissue sample followed by a different loading condition. The initial loading condition was repeated and the results from the repeated conditions showed no differences.

The tissue clamps were designed so that they could be assembled repeatably to minimize differences in the apparent material response of the tissue due to deviations in clamp position. This process is critical when performing repeated material tests on the same tissue sample. The assembly had one fixed clamp and one that moved with the actuator (Fig. 2). Multiple adaptors allowed the same fixed clamp to be used in both tensile and shear configurations. Unique geometries were cut into both the clamp face (where tissue is held) and the stock base of the clamp (where it mates to the test stand) to allow the maintenance of relative clamp position after repeated assembly and disassembly. Adjustments allowed the user to change the rotational orientation between relative clamp faces. Once a given specimen was tested, the overall orientation of the fixed and moving clamps was held constant.

For each tensile elongation (Fig. 2(*a*)), a preload of 0.5 N was applied to the tissue sample using a materials testing machine (Elf 3200, Enduratec, Inc., Eden Prairie, MN) and custom load cell (Honeywell, Morristown, NJ, resolution ± 0.1 N). Once the tissue sample was preloaded, the initial width, length, and thickness of the tissue samples were determined as the average of three measurements obtained using digital calipers (thickness) and a ruler (width and length). The tissue sample was then preconditioned via ten cycles of cyclic elongation to 1.5 mm ($\sim$10% of width) at a rate of 10 mm/min. Preliminary experiments were performed to determine the preload, the appropriate number of cycles of preconditioning, and the preconditioning elongations.

Load-to-failure tests were performed to determine relative values defining the toe and linear regions of the load-elongation curve. To determine the number of cycles required for appropriate preconditioning, the tissue was cyclically loaded until the difference in load-elongation curves between two consecutive loading cycles was minimized (<1 N). A total of ten cycles was capable of achieving this requirement. Directly following preconditioning, a displacement of 2.25 mm ($\sim$15% of width) was applied at a rate of 10 mm/min (which elongated the tissue well into the linear region yet far from the yield point of the tissue—indicated by repeatable curves following the application of this elongation).

Because several nondestructive tests were performed on each tissue sample and the tissue exhibits a strain history, the tissue samples were allowed to recover for 30 min between each test.

The recovery period was chosen based on preliminary tests. A loading condition was applied to a tissue sample and it was then allowed to recover for differing amounts of time. Following recovery, the same loading condition was applied to the tissue sample and the response of the tissue compared. The shortest recovery time required to produce similar results for the two loading curves was found to be 30 min.

Following the recovery period, the tissue sample was removed from the fixed clamp and the tissue that was previously held within the clamps was then reclamped using a shear clamp setup (Fig. 2(*b*)). For shear elongations, two preloads were applied to the tissue sample: one parallel to the axis of loading (0.1 N) using the load cell from the tensile protocol and one perpendicular to the axis of elongation (0.03 N) using an additional load cell (Honeywell, Morristown, NJ, resolution—0.01 N) (Fig. 2(*b*)). Preliminary tests were performed to determine the appropriate preload conditions. When loads less than 0.1 N were applied to the tissue, the loading curve exhibited a drawn out region where zero force was being applied to the tissue, indicating the preloaded was too small. When loads greater than 0.1 N were applied to the tissue, the loading curve became nearly linear, indicating the tissue was excessively preloaded.

Once the tissue was preloaded, the initial width, length, and thickness of the tissue samples were determined as the average of three measurements obtained using digital calipers (thickness) and a ruler (width and length). The tissue sample was then preconditioned via ten cycles of cyclic elongation between 0 mm–2 mm (~8% of height) at a rate of 10 mm/min. Similar to the tensile elongations, preliminary experiments were performed to determine the proper number of cycles of preconditioning as well as preconditioning elongations.

Directly following preconditioning, a displacement equal to a shear ($\kappa = \tan(\theta)$) of 0.4, where θ is the angle between the top edge of the tissue sample and the *x*-axis, was applied at a rate of 10 mm/min (which elongates the tissue well into the linear region yet far from the yield point of the tissue—indicated by repeatable curves following the application of this elongation) [23]. During this test, the load perpendicular to the axis of loading was not held constant, rather the distance between the clamps was held constant. The tissue samples were again allowed to recover for 30 min.

Following the recovery period, the tissue sample was removed from both clamps and the tissue that was previously held within the clamps was carefully dissected away via scalpel transection. The opposite edges of the tissue sample were wrapped in gauze, soaked in saline, and placed in the custom clamps. The tensile and shear protocols were then repeated. From each tensile and shear elongation, the clamp reaction force, tissue sample elongation, and the tissue sample geometry were recorded.

Parameter Optimization. The clamp reaction forces, elongations, and tissue sample geometry (width, thickness, and length measurements) from each experimental loading condition were used as boundary conditions to determine optimal material coefficients for an isotropic hyperelastic strain energy function via an inverse finite element optimization technique [23] (Fig. 3). Only the force in the *y*-direction was used to optimize the material coefficients for the shear loading condition since it was significantly greater than the force in the *x*-direction during loading of the tissue sample. The strain energy was based on the form originally used by Veronda and Westman [24], but with an uncoupled dilatational and deviatoric response [25]:

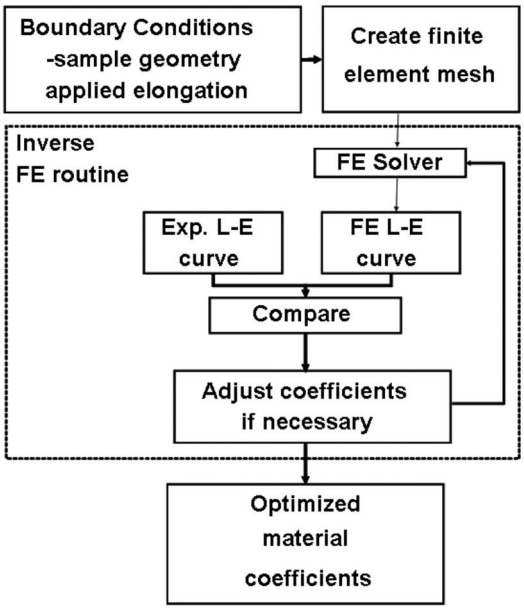

Fig. 3 Flowchart of the inverse finite element methodology [9] utilized to determine the material coefficients for the isotropic constitutive model

$$W = C_1(e^{C_2(\tilde{I}_1-3)} - 1) - \frac{C_1C_2}{2}(\tilde{I}_2 - 3) + U(J) \tag{1}$$

This form of the strain energy represents a material composed of an isotropic matrix. Here, $\tilde{I}_1$ and $\tilde{I}_2$ are the deviatoric invariants of the right Cauchy–Green deformation tensor $\boldsymbol{C}$. $U(J)$ governs the dilational response of the tissue, where J is the volume ratio. Finally, C_1 and C_2 are the material coefficients that were determined using the inverse finite element optimization routine, where C_1 scales the magnitude of the stress-stretch curve and C_2 governs the magnitude and nonlinearity of the stress-stretch curve. This strain energy is convex and exhibits physically reasonable behavior under tension, compression, and shear [23,25].

An image obtained using a high-speed video camera (Adimec, Stoneham, MA; Model 1000 m; resolution=1000×1000 pixels) from each loading condition with the tissue sample in the reference strain configuration, or preloaded state, was used to create a finite element mesh by adjusting nodal points of the mesh until they were aligned with the edges of the tissue samples. Initial estimates for the material coefficients of $C_1=0.1$ and $C_2=10$ were used consistently for the parameter optimization. All finite element calculations were performed using the nonlinear implicitly integrated code NIKE3D [26].

The inverse finite element optimization routine used a sequential quadratic programming method (E04UNF, Numerical Algorithms Group, Oxford, England). The Numerical Algorithms Group (NAG) routine minimized a smooth objective function subject to a set of constraints on the variables:

$$F(C_1, C_2) = \frac{1}{2}\sum_{i=1}^{m} \{y_i - f_i(C_1, C_2)\}^2 \tag{2}$$

Here, $F(C_1, C_2)$ is the objective function, y is the experimental clamp reaction force, $f(C_1, C_2)$ is the clamp reaction force from the finite element simulation, i represents a particular clamp displacement level, and m is the number of discrete clamp displacement levels (11 for this optimization routine, based on previous work performed on the medial collateral ligament (MCL) [27]). Both material coefficients were constrained to be greater than 0 to ensure physically reasonable behavior and strong ellipticity but

Table 1 Tissue sample geometry for tensile longitudinal (TL), tensile transerverse (TT), shear longitudinal (SL), and shear transverse (ST) loading conditions (mean±S.D.)

	TL	TT	SL	ST
Clamp to Clamp (mm)	15.0±0.9	15.2±1.0	15.1±1.2	14.3±1.3
Width (mm)	20.5±4.0	15.0±5.0	16.4±3.0	20.4±3.5
Thickness (mm)	2.0±0.7	4.1±6.3	2.3±0.5	2.1±0.5
Corss sectional area (mm^2)	39.8±16.1	36.7±7.8	37.5±12.8	43.2±15.7

less than 5 (C_1) or 50 (C_2) [28].

The optimized coefficients were then used to generate stress-stretch curves for either uniaxial extension or a simple shear deformation (two stress-stretch curves for uniaxial extension and two stress-stretch curves for simple shear deformation per tissue sample). Each stress-stretch relationship was derived from the appropriate deformation gradient tensor. For uniaxial extension, the deformation gradient and Cauchy stress were

$$F = \begin{bmatrix} \lambda_1 & 0 & 0 \\ 0 & \frac{1}{\sqrt{\lambda_1}} & 0 \\ 0 & 0 & \frac{1}{\sqrt{\lambda_1}} \end{bmatrix} \tag{3}$$

$$T_{11} = \frac{C_1 C_2 (\lambda_1 - 1)(\lambda_1{}^2 + \lambda_1 + 1)(2\lambda_1 e^{C_2(\lambda_1+2)(\lambda_1-1)^2/\lambda_1})}{\lambda_1{}^2} \tag{4}$$

For a simple shear deformation, the deformation gradient and Cauchy stress were

$$F = \begin{bmatrix} 1 & \kappa & 0 \\ 0 & 1 & 0 \\ 0 & 0 & 1 \end{bmatrix} \tag{5}$$

$$T_{12} = \kappa C_1 C_2 (2e^{C_2 \kappa^2} - 1) \tag{6}$$

The stress-stretch curves were discretized into 11 points and averaged across all tissue samples to obtain one stress-stretch curve per loading condition. Thus, a total of four average stress-stretch curves were generated.

To further determine if differences existed in the response of the tissue between the coefficients from each loading condition, the tensile longitudinal stress-stretch curve was compared (using R^2 values) to the tensile transverse stress-stretch curve, and similarly the shear longitudinal stress-stretch curve was compared to the shear transverse stress-stretch curve. Paired t-tests were used to compare the stress values at each of the 11 discretized points. These average stress-stretch curves were then fitted to either the stress-stretch relationship for uniaxial extension (Eq. (4)) or simple shear (Eq. (6)) using the nonlinear Levenberg–Marquardt algorithm to obtain a set of material coefficients for each loading configuration representing the average stress-stretch curves. Based on preliminary analyses to determine the sensitivity of the stress-stretch curves to the material coefficients, changes in the magnitudes of C_1 and C_2 of greater than 0.30 and 3.0, respectively, were considered significant. These changes indicated that the squared correlation coefficient between the two curves was less than 0.97 and the curves would be significantly different.

Results

The cross sectional areas for the tissue samples were 39.8 mm^2 and 36.7 mm^2 for the tensile longitudinal and tensile transverse loading conditions, respectively (Table 1). The cross sectional area for the shear longitudinal tissue samples was 37.5 mm^2, while the cross sectional area for the shear transverse tissue samples was 43.2 mm^2. The clamp to clamp distance was similar for all four loading conditions (approximately 15 mm). The width of the tissue samples was slightly larger for the tensile longitudinal and shear transverse when compared to the tensile transverse and shear longitudinal loading conditions. The thickness of the tissue samples was similar for the tensile longitudinal, shear longitudinal, and shear transverse loading conditions; however, the thickness of the tissue samples for the tensile transverse loading condition was slightly larger. The load-elongation curves for both tensile and shear loadings of each tissue sample exhibited the typical nonlinear upwardly concave shape, including toe regions that progressively became linear (Figs. 4 and 5).

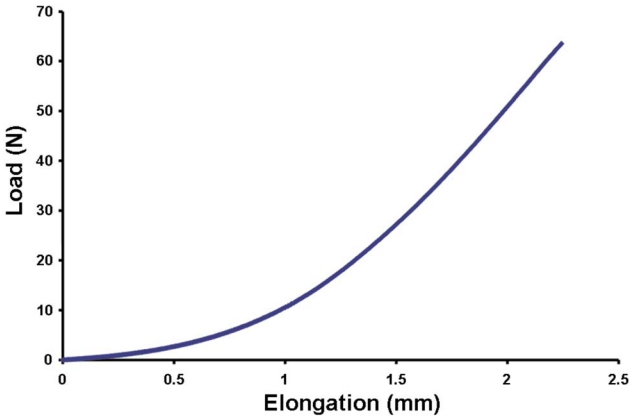

Fig. 4 Representative load-elongation curve of tensile loading condition

No significant differences were found between the material coefficients from the tensile longitudinal and tensile transverse loading conditions (Table 2) based on the previously defined criteria where differences of greater than 0.30 for C_1 and 3.0 for C_2 are considered significant. The C_1 coefficient for the tensile longitudinal loading condition of the axillary pouch ranged from 0.06 MPa to 0.52 MPa, with an average of 0.25±0.17 MPa. The C_2 coefficient for the same loading condition ranged from 5.5 to 17.7, with an average of 11.6±3.8. The C_1 and C_2 coefficients for the tensile transverse loading conditions had similar ranges (C_1 range: 0.06–0.30 MPa; C_2 range: 6.5–17.2) and average values (C_1=0.15±0.07 MPa; C_2=9.7±3.1) compared to the tensile longitudinal loading condition.

Similarly, no significant differences were found between the material coefficients from the shear longitudinal and shear trans-

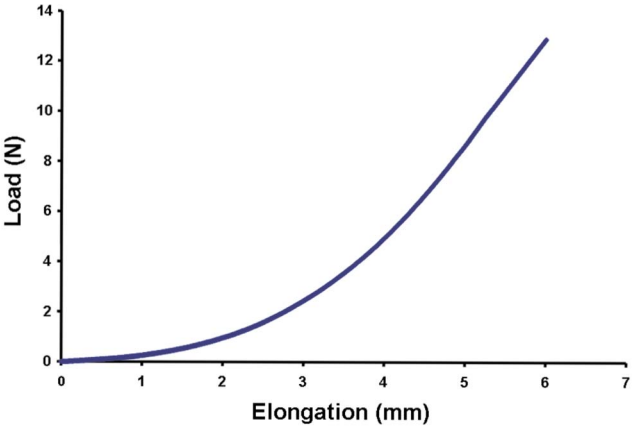

Fig. 5 Representative load-elongation curve of shear loading condition

Table 2 Material coefficients for tissue samples from all specimens

	Specimen 1		Specimen 2		Specimen 3		Specimen 4		Specimen 5		Specimen 6		Specimen 7		Specimen 8		Specimen 9		Specimen 10	
	C_1 (MPa)	C_2	C_1 (MPa)	C_2	C_1 (MPa)	C_2	C_1 (MPa)	C_2	C_1 (MPa)	C_2	C_1 (MPa)	C_2	C_1 (MPa)	C_2	C_1 (MPa)	C_2	C_1 (MPa)	C_2	C_1 (MPa)	C_2
Tensile longitudinal	0.49	8.3	0.52	9.3	0.13	11.7	0.39	5.5	0.06	15.6	0.11	14.5	0.31	8.1	0.12	13.4	0.22	11.8	0.13	17.7
Tensile transverse	0.30	11.3	0.13	6.5	0.24	7.1	0.16	10.3	0.09	11.1	0.12	8.1	0.15	8.8	0.06	8.4	0.13	8.3	0.14	17.2
Shear longitudinal	0.06	10.3	0.83	2.2	0.17	8.4	0.48	3.7	0.09	3.6	0.07	9.1	0.06	10.1	0.05	11.0	0.10	9.3	1.08	2.1
Shear transverse	0.51	3.8	1.78	1.9	0.07	9.5	0.42	3.8	0.20	4.0	0.28	5.6	0.25	5.3	0.11	11.5	0.81	6.3	0.28	7.9

verse loading conditions (Table 2). The C_1 coefficient for the shear longitudinal loading condition of the axillary pouch ranged from 0.05 MPa to 1.08 MPa, with an average of 0.30 ± 0.37 MPa, while the C_2 coefficient for the same loading condition ranged from 2.1 to 11.0, with an average of 7.0 ± 3.6. Similarly, the C_1 and C_2 coefficients for the shear transverse loading conditions had a similar range (C_1 range: 0.07–1.78 MPa; C_2 range 1.9–11.5) and average ($C_1 = 0.47 \pm 0.51$ MPa; $C_2 = 6.0 \pm 2.9$) compared to the shear longitudinal loading condition. However, differences were found when comparing the C_2 coefficients between the tensile and shear loading conditions for several of the individual specimens. For example, the average C_2 coefficients for Specimen 5 were 13.4 for the tensile loading conditions, while the average C_2 coefficients for Specimen 5 were 3.8 for the shear loading conditions.

No statistically significant differences in stress from the stress-stretch curves for uniaxial extension (Fig. 6) or simple shear deformation (Fig. 7) were found ($p > 0.05$). The difference of stress between uniaxial extension in the longitudinal direction and uniaxial extension in the transverse direction of the axillary pouch across all specimens was only 0.46 ± 0.44 MPa. In addition, the correlation coefficients between the curves for uniaxial extension resulting from the material coefficients from the longitudinal and transverse loading conditions exceeded 0.99. Similarly, the difference of stress between the stress-stretch curves for simple shear resulting from the material coefficients for shear longitudinal and transverse loading conditions was only 0.41 ± 0.42 MPa. The correlation coefficients between all stress-stretch curves for simple shear were greater than 0.97.

Finally, no significant differences were found between the material coefficients representing the average stress-stretch curves for uniaxial extension from the tensile longitudinal (C_1:0.21, C_2:11.3) and transverse (C_1:0.13, C_2:11.1) loading conditions. Comparisons were once again made using the criteria from our preliminary sensitivity study (differences of greater than 0.3 for C_1 and 3 for C_2 are considered significant). In addition, no significant differences were found when comparing the material coefficients for simple shear from the shear longitudinal (C_1:0.14, C_2:7.1) and transverse (C_1:0.29, C_2:6.4) loading conditions. Comparison of the C_2 coefficients between the tensile and shear loading conditions reveals significant differences between the values (i.e., 11.3 versus 7.1).

Discussion

In this study a hyperelastic isotropic constitutive model was used to describe the material response of the axillary pouch to tensile and shear loading conditions in two perpendicular directions. No significant differences were found when comparing the material coefficients of the constitutive model between longitudinal and transverse loading directions. In addition, no significant difference was found when comparing the stress-stretch curves between loading directions, thus supporting the hypothesis that isotropy can effectively describe the material symmetry of the glenohumeral capsule.

The results of this study suggest that the material behavior of the glenohumeral capsule under tensile and shear loading can be described by a constitutive model with isotropic symmetry when evaluating the glenohumeral capsule as a sheet of fibrous tissue. The collagen fiber organization of the glenohumeral capsule reported previously [22] supports this finding and further suggests that the interfiber connections within the tissue should remain intact when determining the mechanical or structural properties of different regions of the capsule. In addition, this study characterized the entire stress-stretch curve, including the toe region, instead of just the modulus or stress at failure. During normal activities of daily living, the capsule, and ligaments, in general, are typically only loaded into the toe region. Therefore, this informa-

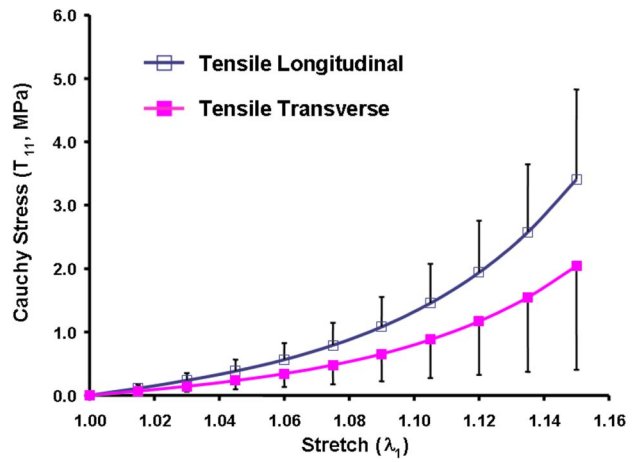

Fig. 6 Average stress-stretch curves for tensile loading conditions

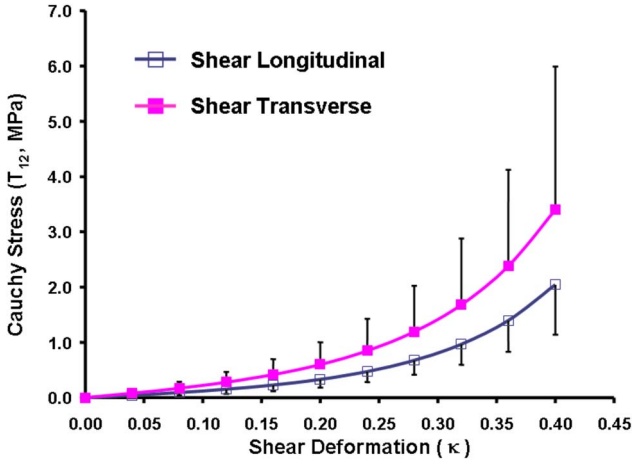

Fig. 7 Average stress-deformation curves for shear loading conditions

tion is important to obtain a thorough understanding of the function of the glenohumeral capsule and improve patient outcomes.

Because a constitutive model like the one used in this study has not been used in any previous studies to describe the material behavior of the glenohumeral capsule, a direct comparison of material coefficients in this study to data in the literature is difficult. Instead, the stresses generated using the optimized coefficients were compared to values reported in the literature. The magnitude of stress from the tensile loading configuration is on the same order of magnitude as the ultimate stress values previously found for the axillary pouch (5.5 MPa) [11] and the posterior capsule (7.9 MPa) [29], even though different experimental protocols were used. Previously, dog-bone samples were excised from the tissue, cutting interfiber connections. The removal of the interfiber connection might have decreased the stress required to fail the tissue, hence the similar values when compared to the current data when the tissue was not loaded to failure.

The assumption of hyperelasticity is implicit in the current constitutive framework. Hyperelasticity provides an appropriate starting point for characterizing the material behavior of the glenohumeral capsule because of its large content of collagen fibers. The assumption of uncoupled deviatoric-dilational response is also commonly employed in finite deformation elasticity for slightly compressible materials [25,28,30]—it greatly decreases the complexity of the constitutive model and finite element implementation. This assumption is justified by the fact that the vast majority of strain energy induced in ligaments is deviatoric because volumetric confinement of the tissue in physiological loading scenarios is minimal. In addition, the material coefficients determined in this study are capable of predicting the response of the axillary pouch to any loading condition and can be implemented in a finite element model of the glenohumeral joint.

The results of this study demonstrate that the isotropic constitutive model can describe the material behavior of the axillary pouch during either tensile or shear loading conditions. However, the material coefficients obtained from tensile loading conditions do not compare well with the material coefficients from the shear loading conditions and only the x-force was used for optimization. Therefore, further work is required to develop a constitutive model that might use force from the x- and y-directions during loading to optimize material coefficients and ultimately predict the response of the tissue samples during tensile and shear loading conditions. The updated constitutive model might also include a random fiber distribution in addition to the homogeneous matrix utilized in this study.

In the future, the material properties of other capsular regions should be determined since the contributions of the entire glenohumeral capsule are important to joint stability. Validated finite element models could then be constructed using these material coefficients and the stress and strain distribution within the glenohumeral capsule could be determined during joint motion. The stress distributions would provide a means for identifying locations within the glenohumeral capsule that are at risk for injury and could be assessed for various joint positions. Moreover, the constitutive coefficients could be altered, simulating changes to the mechanical properties of the capsule due to age, gender, injury, or surgical repair procedures, such as thermocapsular shrinkage [31,32].

Acknowledgment

The authors would like to acknowledge the funding support of NIH Grant Nos. R01-AR050218 and R01-AR047369, as well as the contributions of Benjamin Ellis and Elizabeth Timcho.

References

[1] DePalma, A. F., Callery, G., and Bennett, G. A., 1949, "Variational Anatomy and Degenerative Lesions of the Shoulder Joint," American Academy of Orthopaedic Surgery Instructional Course Lecture Series, **6**, pp. 225–281.

[2] O'Brien, S. J., Arnoczsky, S. P., Warren, R. F., and Rozbruch, S. R., 1990, "Developmental Anatomy of the Shoulder and Anatomy of the Glenohumeral Joint," *The Shoulder*, F. A. Matsen, III, and C. A. Rockwood, eds., W. B. Saunders Co., Philadelphia, PA, pp. 1–33.

[3] Turkel, S. J., Panio, M. W., Marshall, J. L., and Girgis, F. G., 1981, "Stabilizing Mechanisms Preventing Anterior Dislocation of the Glenohumeral Joint," J. Bone Jt. Surg., Am. Vol., **63**(8), pp. 1208–1217.

[4] Warner, J. J. P., Caborn, D. N., Berger, R., Fu, F. H., and Seel, M., 1993, "Dynamic Capsuloligamentous Anatomy of the Glenohumeral Joint," J. Shoulder Elbow Surg., **2**, pp. 115–133.

[5] Malicky, D. M., Soslowsky, L. J., Blasier, R. B., and Shyr, Y., 1996, "Anterior Glenohumeral Stabilization Factors: Progressive Effects in a Biomechanical Model," J. Orthop. Res., **14**(2), pp. 282–288.

[6] Novotny, J. E., Beynnon, B. D., and Nichols, C. E., 2000, "Modeling the Stability of the Human Glenohumeral Joint During External Rotation," J. Biomech., **33**(3), pp. 345–354.

[7] Debski, R. E., Wong, E. K., Woo, S. L., Fu, F. H., and Warner, J. J., 1999, "An Analytical Approach to Determine the In Situ Forces in the Glenohumeral Ligaments," ASME J. Biomech. Eng., **121**(3), pp. 311–315.

[8] Malicky, D. M., Soslowsky, L. J., Kuhn, J. E., Bey, M. J., Mouro, C. M., Raz, J. A., and Liu, C. A., 2001, "Total Strain Fields of the Antero-Inferior Shoulder Capsule Under Subluxation: A Stereoradiogrammetric Study," ASME J. Biomech. Eng., **123**(5), pp. 425–431.

[9] Malicky, D. M., Kuhn, J. E., Frisancho, J. C., Lindholm, S. R., Raz, J. A., and Soslowsky, L. J., 2002, "Neer Award 2001: Nonrecoverable Strain Fields of the Anteroinferior Glenohumeral Capsule Under Subluxation," J. Shoulder Elbow Surg., **11**(6), pp. 529–540.

[10] Debski, R. E., Wong, E. K., Woo, S. L.-Y., Sakane, M., Fu, F. H., and Warner, J. J., 1999, "In Situ Force Distribution in the Glenohumeral Joint Capsule During Anterior-Posterior Loading," J. Orthop. Res., **17**(5), pp. 769–776.

[11] Bigliani, L. U., Pollock, R. G., Soslowsky, L. J., Flatow, E. L., Pawluk, R. J., and Mow, V. C., 1992, "Tensile Properties of the Inferior Glenohumeral Ligament," J. Orthop. Res., **10**(2), pp. 187–197.

[12] Itoi, E., Grabowski, J. J., Morrey, B. F., and An, K. N., 1993, "Capsular Properties of the Shoulder," Tohoku J. Exp. Med., **171**(3), pp. 203–210.

[13] Boardman, N. D., Debski, R. E., Warner, J. J., Taskiran, E., Maddox, L., Imhoff, A. B., Fu, F. H., and Woo, S. L.-Y., 1996, "Tensile Properties of the Superior Glenohumeral and Coracohumeral Ligaments," J. Shoulder Elbow Surg., **5**(4), pp. 249–254.

[14] Ticker, J. B., Bigliani, L. U., Soslowsky, L. J., Pawluk, R. J., Flatow, E. L., and Mow, V. C., 1996, "Inferior Glenohumeral Ligament: Geometric and Strain-Rate Dependent Properties," J. Shoulder Elbow Surg., **5**(4), pp. 269–279.

[15] McMahon, P. J., Tibone, J. E., Cawley, P. W., Hamilton, C., Fechter, J. D., Elattrache, N. S., and Lee, T. Q., 1998, "The Anterior Band of the Inferior Glenohumeral Ligament: Biomechanical Properties From Tensile Testing in the Position of Apprehension," J. Shoulder Elbow Surg., **7**(5), pp. 467–471.

[16] Stefko, J. M., Tibone, J. E., Cawley, P. W., ElAttrache, N. E., and McMahon, P. J., 1997, "Strain of the Anterior Band of the Inferior Glenohumeral Ligament During Capsule Failure," J. Shoulder Elbow Surg., **6**(5), pp. 473–479.

[17] Reeves, B., 1968, "Experiments on the Tensile Strength of the Anterior Capsular Structures of the Shoulder in Man," J. Bone Jt. Surg., Br. Vol., **50**(4), pp. 858–865.

[18] Moore, S. M., McMahon, P. J., and Debski, R. E., 2004, "Bi-Directional Mechanical Properties of the Axillary Pouch of the Glenohumeral Capsule: Implications for Surgical Repair," ASME J. Biomech. Eng., **126**(2), pp. 284–288.

[19] Moore, S. M., McMahon, P. J., Azemi, E., and Debski, R. E., 2005, "Bi-Directional Mechanical Properties of the Posterior Region of the Glenohumeral Capsule," J. Biomech., **38**(6), pp. 1365–1369.

[20] Gohlke, F., Essigkrug, B., and Schmitz, F., 1994, "The Patterns of the Collagen Fiber Bundles of the Capsule of the Glenohumeral Joint," J. Shoulder Elbow Surg., **3**(3), pp. 111–128.

[21] O'Brien, S. J., Neves, M. C., Arnoczky, S. P., Rozbruck, S. R., Dicarlo, E. F., Warren, R. F., Schwartz, R., and Wickiewicz, T. L., 1990, "The Anatomy and Histology of the Inferior Glenohumeral Ligament Complex of the Shoulder," Am. J. Sports Med., **18**(5), pp. 449–456.

[22] Debski, R. E., Moore, S. M., Mercer, J. L., Sacks, M. S., and McMahon, P. J., 2003, "The Collagen Fibers of the Anteroinferior Capsulolabrum Have Multi-Axial Orientation to Resist Shoulder Dislocation," J. Shoulder Elbow Surg., **12**, pp. 247–252.

[23] Weiss, J. A., Gardiner, J. C., and Bonifasi-Lista, C., 2002, "Ligament Material Behavior is Nonlinear, Viscoelastic and Rate-Independent Under Shear Loading," J. Biomech., **35**(7), pp. 943–950.

[24] Veronda, D. R., and Westmann, R. A., 1970, "Mechanical Characterization of Skin-Finite Deformations," J. Biomech., **3**, pp. 111–124.

[25] Weiss, J. A., Maker, B. N., and Govindjee, S., 1996, "Finite Element Implementation of Incompressible, Transversely Isotropic Hyperelasticity," Comput. Methods Appl. Mech. Eng., **135**, pp. 107–128.

[26] Maker, B. N., Ferencz, R. M., and Hallquist, J. O., 1990, "NIKE3D: A Nonlinear, Implicit, Three-Dimensional Finite Element Code for Solid and Structural Mechanics," Lawrence Livermore National Laboratory, Technical Report No. UCRL-MA-105268.

[27] Gardiner, J. C., and Weiss, J. A., 2001, "Simple Shear Testing of Parallel-Fibered Planar Soft Tissues," J. Biomech., **123**, pp. 1–5.

[28] Marsden, J. E., and Hughes, T. J. R., 1994, "Mathematical Foundations of Elasticity," Dover, New York.

[29] Bey, M. J., Hunter, S. A., Kilambi, N., Butler, D. L., and Lindenfeld, T. N., 2005, "Structural and Mechanical Properties of the Glenohumeral Joint Posterior Capsule," J. Shoulder Elbow Surg., **14**(2), pp. 201–206.
[30] Simo, J. C., 1988, "On the Dynamics in Space of Rods Undergoing Large Motions: A Geometrically Exact Approach," Comput. Methods Appl. Mech. Eng., **66**, pp. 125–161.
[31] Chen, S., Haen, P. S., Walton, J., and Murrell, G. A., 2005, "The Effects of Thermal Capsular Shrinkage on the Outcomes of Arthroscopic Stabilization for Primary Anterior Shoulder Instability," Am. J. Sports Med., **33**(5), pp. 705–711.
[32] Levine, W. N., Bigliani, L. U., and Ahmad, C. S., 2004, "Thermal Capsulorrhaphy," Orthopedics, **27**(8), pp. 823–826.